Am J Cancer Res 2023;13(10):4693-4707
www.ajcr.us /ISSN:2156-6976/ajcr0151978

Original Article

Development of triazole-based PKC-inhibitors to overcome resistance to EGFR inhibitors in EGFR-mutant lung cancers

Pei-Chih Lee[1,2,3*], Vathan Kumar[4,5*], Govindan Sivakumar[4,5,6*], Tzu-Yu Tseng[1,2,3], Yi-Chuan Li[7], Yu-Cyuan Jiang[1,2,3], Yu-Chun Hsiao[1,2,3], Hsiang-Wen Lin[4,5], Chih-Shiang Chang[4,5], Mien-Chie Hung[1,2,3,8,9]

[1]Graduate Institute of Biomedical Sciences, China Medical University, Taichung, Taiwan; [2]Research Center for Cancer Biology, China Medical University, Taichung, Taiwan; [3]Cancer Biology and Precision Therapeutics Center, China Medical University, Taichung, Taiwan; [4]School of Pharmacy, College of Pharmacy, China Medical University, Taichung, Taiwan; [5]Drug Development Center, China Medical University, Taichung, Taiwan; [6]Graduate Institute of Biomedical Engineering, National Chung Hsing University, Taichung, Taiwan; [7]Department of Biological Science and Technology, College of Life Sciences, China Medical University, Taichung, Taiwan; [8]Institute of Biochemistry and Molecular Biology, College of Life Sciences, China Medical University, Taichung, Taiwan; [9]Center for Molecular Medicine, China Medical University Hospital, China Medical University, Taichung, Taiwan. [*]Equal contributors.

Received June 29, 2023; Accepted August 22, 2023; Epub October 15, 2023; Published October 30, 2023

Abstract: Protein kinase C delta (PKCδ) is prominently expressed in the nuclei of EGFR-mutant lung cancer cells, and its presence correlates with poor survival of the patients undergoing EGFR inhibitor treatment. The inhibition of PKCδ has emerged as a viable approach to overcoming resistance to EGFR inhibitors. However, clinical-grade PKCδ inhibitors are not available, highlighting the urgent needs for the development of effective drugs that target PKCδ. In this study, we designed and synthesized a series of inhibitors based on the chemical structure of a pan PKC inhibitor sotrastaurin. This was achieved by incorporating a triazole ring group into the original sotrastaurin configuration. Our findings revealed that the sotrastaurin derivative CMU-0101 exhibited an elevated affinity for binding to the ATP-binding site of PKCδ and effectively suppressed nuclear PKCδ in resistant cells in comparison to sotrastaurin. Furthermore, we demonstrated that CMU-0101 synergistically enhanced EGFR TKI gefitinib sensitivity in resistant cells. Altogether, our study provides a promising strategy for designing and synthesizing PKCδ inhibitors with improved efficacy, and suggests CMU-0101 as a potential lead compound to inhibit PKCδ and overcome TKI resistance in lung cancers.

Keywords: Protein kinase C, PKC inhibitor, EGFR, resistance, lung cancer

Introduction

Lung cancer is characterized by a heterogeneous disease, marked by significant genomic instability and diversity. The epidermal growth factor receptor (EGFR) gene frequently undergoes mutations in non-small cell lung cancers (NSCLCs), making EGFR-activating mutations pivotal oncogenic drivers. This has led to a biomarker-guided treatment approach for advanced-stage NSCLC patients through the use of EGFR tyrosine kinase inhibitors (TKIs) [1]. Despite their initial success, TKIs are hampered by the emergence of heterogeneous resistance mechanisms within lung tumors, ultimately undermining their efficacy over time [2]. Individual patients often manifest diverse resistance mechanisms, such as the acquisition of additional EGFR mutations and upregulation of multiple receptor tyrosine kinases (RTKs). This diversity renders the combination therapy of a single RTK inhibitor with TKIs ineffective [3-5]. The emergence of resistance to TKIs remains a significant challenge in the treatment of NSCLCs.

Protein kinases are vital enzymes that regulate various cellular processes by phosphorylating their substrates. Protein kinase C (PKC) is a family of serine/threonine kinases that play important roles in signal transduction, cell proliferation, differentiation, and apoptosis [6, 7].

In lung cancers, the nuclear localization of PKC delta (nPKCδ) has emerged as a common resistant mediator across various known TKI-resistant pathways [8]. nPKCδ is actively expressed in a significant portion of TKI-resistant patients and is associated with poor survival in EGFR-mutant patients treated with TKIs [8]. The nPKCδ-mediated pathway, including AKT [9] and NF-kB [10], has been implicated in promoting resistance to EGFR inhibitors by activating alternative survival signaling pathways that bypass the blocked EGFR signaling and bolster tumor growth. Our research has demonstrated that specific shRNA-mediated inhibition of nPKCδ sensitizes TKI-resistant cells to TKIs [8]. Additionally, commercially available pan-PKC inhibitors like sotrastaurin have been employed as proof-of-concept treatments to surmount TKI resistance in preclinical models [8]. Consequently, targeting nPKCδ presents a promising way for addressing the heterogeneous mechanisms of TKI resistance in NSCLCs.

Despite this progress, clinical-grade PKCδ inhibitors are currently lacking, resulting the urgent need for drugs designed to effectively target PKCδ, potentially overcoming TKI resistance in lung cancers. In this study, we adopted a hybridization strategy [11] to synthesize and develop novel small molecule PKC inhibitors based on the sotrastaurin structure. This involved combining two or more bioactive pharmacophores such as indole, quinazoline, and triazole moieties. As a result, we synthesized five sotrastaurin derivatives CMU-0101, 0102, 0103, 0104, and 0105, and assessed their anti-cancer efficacy. Our investigations disclosed that among these derivatives, CMU-0101 exhibited the most potent inhibition of nPKCδ. Notably, the combination of CMU-0101 with EGFR TKIs synergistically suppressed cell growth in TKI-resistant lung cancer cells. Our study highlights the potential of the quinazolinyl-indolyl-triazole based hybrid molecules as a promising strategy for developing potent PKC inhibitors. Importantly, we demonstrated that CMU-0101 effectively counteracted resistance to TKI in EGFR-mutant lung cancer cells.

Material and methods

Cell culture

Human NSCLC HCC827 cell line were obtained from ATCC and were grown in RPMI medium supplemented with 10% fetal bovine serum (FBS). HCC827 gefitinib-resistant cells (GR cells) were in standard RPMI medium in the presence of 1 μM gefitinib. All the cells have been tested for mycoplasma contamination and were validated by short tandem repeat (STR) DNA fingerprinting as described previously [8].

Cell viability assays

Cellular responses to the treatments were estimated by MTT assay or Crystal violet staining as described previously [8]. The median inhibitory concentration for each drug was determined from the dose-effect relationship and the interactions of two drug treatments were evaluated by the Chou-Talalay combination indices [12] using the CompuSyn software (version 1.0.1; CompuSyn, Inc.).

Confocal microscopy analysis

Confocal microscopy analysis was performed as described previously [8]. Briefly, drug-treated cells were washed with PBS and fixed in cold 100% methanol for 20 min. Cells were then subjected to permeabilization with 3% bovine serum albumin overnight at 4°C. After that, cells were incubated with primary antibodies overnight at 4°C, washed with PBS and further incubated with the appropriate secondary antibody. Nuclei were counterstained with 4,6-diamidino-2-phenylindole (DAPI) before mounting. Confocal fluorescence images were captured and the fluorescence intensity were analyzed by ImageXpress Micro confocal system (Molecular Devices).

WB analysis and antibodies

The Western blot (WB) analysis was conducted as described previously [13]. In summary, cells were subjected to two washes with PBS, followed by lysis in lysis buffer. Subsequently, proteins were separated using SDS electrophoresis on polyacrylamide gels. These proteins were then transferred onto Immun-Blot PVDF membrane (Bio-rad). Following an incubation with the primary antibody, the blots underwent a thorough washing step before being exposed to secondary antibodies. The developed blots were visualized using an iBright imaging system (Thermo Fisher Scientific). The following were the antibodies used: anti-mouse tubulin (Genetex, GTX27291), anti-rabbit Histone-H3 (Proteintech, 17168-1-AP), anti-rabbit PKCδ (Abcam, ab182126), anti-rabbit phospho-PKCδ (Thr505) (Cell signaling, 9374), anti-rabbit

phospho-PKCε (Ser729) (Genetex, GTX1339-37), anti-rabbit phospho-PKCη (Thr655) (Genetex, GTX25798), anti-rabbit phospho-PKCθ (Thr538) (Cell signaling, 9377).

Molecular docking of PKCδ and ligands

Prediction of PKCδ structure was accomplished by AlphaFold version 2.3.2. [14, 15]. The model with highest pLDDT score was used for docking analysis [16]. The crystal structure of PKCα in complex with sotrastaurin with resolution 2.80 Å (PDB ID: 3IW4 [17]) was obtained from the Protein Data Bank (https://www.rcsb.org/). We aligned PKCα to PKCδ using PyMOL Molecular Graphics System, version 2.3 Schrö̈dinger, LL and identified the sotrastaurin binding site with a radius of 8.0 Å.

The 3D structures of sotrastaurin and CMU-0101 were downloaded and drew from the PubChem database (https://pubchem.ncbi.nlm.nih.gov/accessed on 29 December 2022), respectively, and were converted into MOL files using Online SMILES Translator and Structure File Generator (https://cactus.nci.nih.gov/translate/). Docking tasks were performed using AutoDock Vina software [18]. After docking, the conformation with the lowest binding energy was chosen for analysis. Protein structure graphic figures were generated by PyMOL Molecular Graphics System, version 2.3 Schrödinger, LL. Docking results were visualized using LigPlot+ v.2.2.5 [19].

Synthesis and development of triazole-based PKC-inhibitors

To synthesize and develop the new sotrastaurin derivatives by combining two or more bioactive pharmacophores (including indole, quinazoline, and triazole moieties), triazole-based derivatives was considered as the most efficient and appropriate compounds. Compounds 4a-c were synthesized following some parts of the reported methods [20, 21].

Ethyl 3-((2-chloroquinazolin-4-yl) ethynyl)-1H-indole-1-carboxylate (7a): A 25 mL round bottom flask was charged with 5a (0.13 g, 0.43 mmol), bis(triphenylphosphine)palladium(II) chloride (35 mg, 0.5 mmol) and copper iodide (5 mg, 0.03 mmol) and placed under argon. A 3 mL solution of 6:1 (v/v) Et_3N/DMF was added, followed by 1 mL increments of DMF until complete dissolution. A sample of 2,4-dichloroquinazoline (0.2 g, 10.1 mmol) was dissolved in 0.5 mL DMF and added to the reaction mixture, and the resulting solution was warmed at 45°C. After 3 h, the reaction mixture became a heterogeneous opaque orange color, at which point the reaction was removed from heat and collected over a Celite pad. The residue was washed with EtOAc before being dissolved and filtered through the Celite with CH_2Cl_2. The filtrate was concentrated under reduced pressure to give 6a as a white powder 62% yield. ^{1}H NMR (400 MHz, d-d_6) δ 1.45 (t, J = 7.2 Hz, 3H), 4.52 (qr, J = 7.2 Hz, 2H), 7.44-7.52 (m, 2H), 7.84 (d, 7.48 Hz, 1H), 7.89 (t, J = 7.44 Hz, 1H), 7.98 (d, J = 8.4 Hz, 1H), 8.12-8.16 (m, 2H), 8.53 (d, J = 8.2 Hz, 1H), 8.59 (s, 1H). ^{13}C NMR (100 MHz, DMSO-d_6) δ 14.51, 64.68, 89.05, 94.07, 100.75, 115.77, 120.22, 123.49, 124.76, 126.49, 127.24, 127.85, 129.46, 129.96, 134.42, 134.62, 136.74, 150.02, 151.80, 154.89, 156.45.

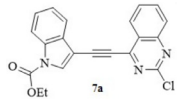

7a

Ethyl 3-(5-(2-chloroquinazolin-4-yl)-2H-1,2,3-triazol-4-yl)-1H-indole-1-carboxylate (8a): A solution of 6a (0.05 g, 1.32 mmol) in DMSO (5 mL) at room temperature was treated with sodium azide (0.013 g, 2.03 mmol) for 3 h. After the completion of the reaction, as indicated by TLC, the reaction mixture was diluted with water and extracted with ethyl acetate. The combined organic layer was washed with brine and dried over anhydrous Na_2SO_4. The organic layer was concentrated and purified by flash column chromatography, using Ethylacetate-hexane (30%) to afford the pure product as a pale yellow solid 7a in 96% yield. ^{1}H NMR (400 MHz, DMSO-d_6) δ 1.43 (t, J = 7.12 Hz, 3H), 4.48 (qr, J = 7.12 Hz, 2H), 7.29-7.33 (m, 1H), 7.36-7.40 (m, 1H), 7.75-7.79 (m, 1H), 7.95-7.97 (m, 1H), 8.02-8.06 (m, 1H), 8.18 (d, J = 8.16 Hz, 1H), 8.27 (d, J = 7.72 Hz, 1H), 8.81 (s, 1H), 9.15 (d, J = 7.96 Hz, 1H). ^{13}C NMR (100 MHz, DMSO-d_6) δ 14.71, 63.80, 112.63, 114.90, 121.82, 122.89, 123.53, 125.14, 126.25, 127.57, 128.66, 129.64, 129.72, 135.27, 135.56, 139.77, 140.17, 150.77, 150.88, 155.97, 163.30.

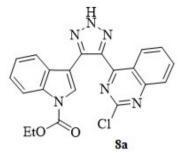

8a

4-(5-(1H-indol-3-yl)-2H-1,2,3-triazol-4-yl)-2-(4-methylpiperazin-1-yl)quinazoline (10a, CMU-0101): A using ethyl3-(5-(2-chloroquinazolin-4-yl)-2H-1,2,3-triazol-4-yl)-1H-indole-1-carboxylate (7a, 0.042 g, 0.1 mmol), *N*-methylpiperazine (0.011 g, 0.11 mmol) in isopropylalcohol (5 mL) at room temperature. The reaction mixture was refluxed for overnight. After the completion of the reaction, as indicated by TLC, the reaction mixture was concentrated, and the resulting crude mass was diluted with water and extracted with ethyl acetate. The combined organic layer was washed with brine and dried over anhydrous Na_2SO_4. The organic layer was concentrated crud product (8a) was taken into the next step hydrolyzed of an ester group by using LiOH (26 mg, 0.12 mmol) in methanol (5 mL) at room temperature. The reaction mixture was stirred at room temperature for 12 h. After the completion of the reaction, as indicated by TLC, the reaction mixture was concentrated, and the resulting crude mass was diluted with water and extracted with ethyl acetate. The combined organic layer was washed with brine and dried over anhydrous Na_2SO_4. The organic layer was concentrated and purified by flash column chromatography, using Methanol-DCM (2:8) to afford the pure product as a pale yellow solid 9a in 88% yield. ^{1}H NMR (400 MHz, CD_3OD) δ 2.17 (d, J = 4.4 Hz, 4H), 2.23 (s, 3H), 3.55 (brs, 4H), 6.90-6.94 (m, 1H), 7.11-7.15 (m, 2H), 7.24-7.28 (m, 1H), 7.42-7.44 (m, 1H), 7.56 (s, 1H), 7.60 (d, J = 8.16 Hz, 1H), 7.69-7.74 (m, 1H), 8.48 (dd, J = 0.92 Hz, J = 0.96 Hz, 1H). ^{13}C NMR (100 MHz, CD_3OD) δ 42.74, 44.54, 54.07, 103.73, 111.36, 117.80, 119.37, 119.57, 121.79, 122.57, 124.66, 125.37, 125.41, 127.48, 133.80, 136.68, 137.87, 140.02, 153.46, 157.94, 160.49. MS (*m/z*) 411 (M^++1).

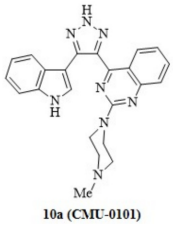

10a (CMU-0101)

Ethyl 5-fluoro-3-iodo-1H-indole-1-carboxylate (3b): Yield 75%, ^{1}H NMR (400 MHz, $CDCl_3$) δ 1.47 (t, J = 7.12 Hz, 3H), 4.49 (q, J = 7.12 Hz, 2H), 7.05-7.13 (m, 2H), 7.63-7.80 (m, 1H), 8.10 (brs, 1H). ^{13}C NMR (100 MHz, $CDCl_3$) δ 14.37, 63.75, 65.19, 65.23, 107.20, 107.45, 113.34, 113.59, 116.23, 116.32, 131.22, 133.40, 149.76, 158.64, 161.03.

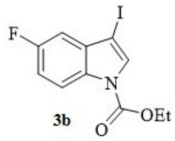

3b

Ethyl 5-fluoro-3-((trimethylsilyl)ethynyl)-1H-indole-1-carboxylate (4b): Yield 78%, ^{1}H NMR (400 MHz, $CDCl_3$) δ 0.29 (t, J = 3.6 Hz, 9H), 1.46 (t, J = 7.2 Hz, 3H), 4.48 (q, J = 7.2 Hz, 2H), 7.06-7.11 (m, 1H), 7.31 (dd, J = 2.8 Hz, 2.8 Hz, 1H), 7.83 (s, 1H), 8.08-8.11 (m, 1H). ^{13}C NMR (100 MHz, $CDCl_3$) δ 0.03, 14.33, 63.75, 95.78, 99.02, 104.01, 104.05, 105.80, 106.04, 113.18, 113.43, 116.24, 116.33, 130.89, 131.58, 131.68, 150.16, 158.59, 160.98.

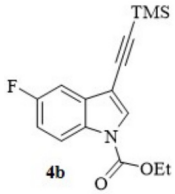

4b

Ethyl 3-ethynyl-5-fluoro-1H-indole-1-carboxylate (5b): Yield 78%, ^{1}H NMR (400 MHz, $CDCl_3$) δ 1.47 (t, J = 7.2 Hz, 3H), 3.26 (s, 1H), 4.50 (q, J = 7.2 Hz, 2H), 7.07-7.12 (m, 1H), 7.33 (dd, J = 2.8 Hz, 2.8 Hz, 1H), 7.86 (s, 1H), 8.09-8.12 (m, 1H). ^{13}C NMR (100 MHz, $CDCl_3$) δ 14.36, 63.84, 74.95, 81.35, 102.87, 102.90, 105.69, 105.94, 113.30, 113.55, 116.33, 116.42, 130.77, 130.88, 131.50, 131.60, 150.12, 158.62, 161.02.

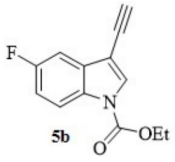

5b

Ethyl 3-((2-chloroquinazolin-4-yl)ethynyl)-5-fluoro-1H-indole-1-carboxylate (7b): Yield 83%, ^{1}H NMR (400 MHz, $CDCl_3$) δ 1.52 (t, J = 7.2 Hz, 3H), 4.56 (q, J = 7.2 Hz, 2H), 7.15-7.20 (m, 1H), 7.52 (dd, J = 2.4 Hz, 2.4 Hz, 1H), 7.75-7.79 (m, 1H), 7.96-8.02 (m, 2H), 8.18-8.20 (m, 2H), 8.39-8.42 (m, 2H). ^{13}C NMR (100 MHz, $CDCl_3$) δ 14.34, 64.38, 89.01, 92.81, 101.69, 105.90, 106.15, 113.99, 114.24, 116.78, 116.87, 123.47, 126.55, 128.05, 128.72, 130.71,

130.81, 131.13, 133.31, 135.53, 149.82, 152.03, 154.88, 157.13, 158.88, 162.29.

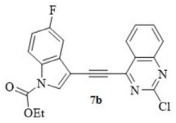

Ethyl 3-(5-(2-chloroquinazolin-4-yl)-2H-1,2,3-triazol-4-yl)-5-fluoro-1H-indole-1-carboxylate (8b): Yield 95%, ^{1}H NMR (400 MHz, DMSO-d_6) δ 1.43 (t, J = 7.2 Hz, 3H), 4.49 (q, J = 7.2 Hz, 2H), 7.26-7.31 (m, 1H), 7.82-7.86 (m, 2H), 8.05 (d, J = 8 Hz, 1H), 8.11-8.15 (m, 1H), 8.17-8.20 (m, 1H), 8.81 (m, 1H), 8.84 (brs, 1H). ^{13}C NMR (100 MHz, DMSO-d_6) δ 14.62, 64.26, 107.75, 113.16, 113.41, 116.46, 116.55, 121.74, 127.95, 128.59, 129.01, 129.48, 131.72, 136.31, 150.40, 153.04, 155.64, 161.88.

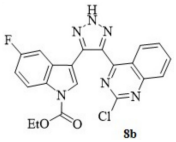

Ethyl 3-iodo-5-methyl-1H-indole-1-carboxylate (3c): Yield 82%, ^{1}H NMR (400 MHz, $CDCl_3$) δ 1.47 (t, J = 7.2 Hz, 3H), 4.48 (q, J = 7.2 Hz, 2H), 7.19 (d, J = 7.2 Hz, 2H), 7.73 (s, 1H), 8.01 (d, J = 8 Hz, 1H). ^{13}C NMR (100 MHz, $CDCl_3$) δ 14.42, 21.35, 63.47, 66.09, 114.73, 121.42, 126.96, 129.70, 132.19, 133.01, 133.32, 150.06.

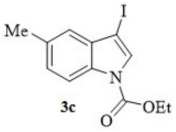

Ethyl 5-methyl-3-((trimethylsilyl)ethynyl)-1H-indole-1-carboxylate (4c): Yield 85%, ^{1}H NMR (400 MHz, $CDCl_3$) δ 0.30 (s, 9H), 1.46 (t, J = 7.2 Hz, 3H), 2.48 (s, 3H), 4.47 (q, J = 7.2 Hz, 2H), 7.18 (dd, J = 1.2 Hz, 1.2 Hz, 1H), 7.45 (s, 1H), 7.78 (s, 1H), 8.01 (d, J = 8 Hz, 1H). ^{13}C NMR (100 MHz, $CDCl_3$) δ 0.12, 14.37, 21.34, 63.47, 96.70, 98.25, 103.84, 114.80, 120.04, 126.76, 129.17, 130.63, 132.77, 133.13, 150.42.

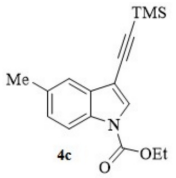

Ethyl 3-ethynyl-5-methyl-1H-indole-1-carboxylate (5c): Yield 98%, ^{1}H NMR (400 MHz, $CDCl_3$) δ 1.47 (t, J = 7.2 Hz, 3H), 2.47 (s, 3H), 3.25 (s, 1H), 4.49 (q, J = 7.2 Hz, 2H), 7.19 (dd, J = 1.6 Hz, 1.6 Hz, 1H), 7.47 (t, J = 0.4 Hz, 1H), 7.81 (s, 1H), 8.02 (d, J = 8 Hz, 1H). ^{13}C NMR (100 MHz, $CDCl_3$) δ 14.37, 21.31, 63.56, 75.76, 80.77, 102.69, 114.88, 119.94, 126.84, 129.55, 130.62, 132.75, 133.25, 150.40.

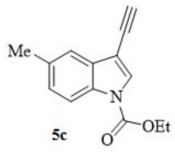

Ethyl 3-((2-chloroquinazolin-4-yl)ethynyl)-5-methyl-1H-indole-1-carboxylate (7c): Yield 79%, ^{1}H NMR (400 MHz, $CDCl_3$) δ 1.51 (t, J = 7.2 Hz, 3H), 2.53 (s, 3H), 4.55 (q, J = 7.2 Hz, 2H), 7.25-7.27 (m, 1H), 7.65 (t, J = 0.8 Hz, 1H), 7.23-7.77 (m, 1H), 7.94-8.01 (m, 2H), 8.07 (d, J = 8.4 Hz, 1H), 8.11 (s, 1H), 8.42-8.45 (m, 1H). ^{13}C NMR (100 MHz, $CDCl_3$) δ 14.37, 21.41, 64.07, 88.70, 94.19, 101.54, 115.18, 120.13, 123.55, 126.74, 127.44, 127.99, 128.55, 129.83, 132.15, 132.96, 133.97, 135.41, 150.10, 151.98, 155.17, 157.16.

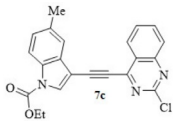

Ethyl 3-(5-(2-chloroquinazolin-4-yl)-2H-1,2,3-triazol-4-yl)-5-methyl-1H-indole-1-carboxylate (8c): Yield 96%, ^{1}H NMR (400 MHz, DMSO-d_6) δ 1.42 (t, J = 7.2 Hz, 3H), 2.41 (s, 3H), 4.47 (t, J = 7.2 Hz, 2H), 7.23 (dd, J = 1.6 Hz, 1.6 Hz, 1H), 7.80-7.84 (m, 1H), 7.93 (brs, 1H), 8.01-8.05 (m, 2H), 8.08-8.12 (m, 1H), 8.70 (s, 1H), 8.89 (d, J = 8.4 Hz, 1H). ^{13}C NMR (100 MHz, DMSO-d_6) δ 14.71, 21.60, 63.75, 114.57, 121.85, 122.64, 126.42, 127.60, 128.81, 129.56, 129.74, 132.52, 133.48, 135.72, 139.66, 150.75, 152.84, 155.93, 163.32.

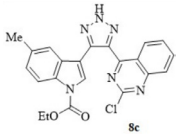

N^1-(4-(5-(1H-indol-3-yl)-2H-1,2,3-triazol-4-yl) quinazolin-2-yl)-N^2,N^2-dimethylethane-1,2-diamine (10b, CMU-0102): Yield 86%, ^{1}H NMR

(400 MHz, CD_3OD) δ 2.58 (brs, 6H), 2.87 (brs, 2H), 3.54 (brs, 2H), 6.97 (t, *J* = 7.72 Hz, 1H), 7.12-7.22 (m, 2H), 7.41-7.43 (m, 2H), 7.58-7.62 (m, 2H), 7.70-7.74 (m, 1H), 8.11 (brs, 1H). ^{13}C NMR (100 MHz, CD_3OD) δ 37.96, 44.32, 57.39, 103.95, 112.28, 118.92, 120.18, 120.51, 122.24, 122.79, 125.90, 126.60, 127.94, 134.54, 136.54, 139.16, 159.13, 161.93. MS (*m/z*) 399 (M^++1).

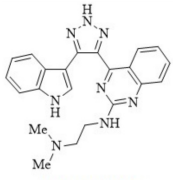

10b (CMU-0102)

N^1-(4-(5-(1H-indol-3-yl)-2H-1,2,3-triazol-4-yl) quinazolin-2-yl)-N^3,N^3-dimethylpropane-1,3-diamine (10c, CMU-0103): Yield 87%, ^1H NMR (400 MHz, CD_3OD) δ 1.80 (brs, 2H), 2.39 (s, 6H), 2.63 (t, *J* = 14.4 Hz, 2H), 3.38 (brs, 2H), 6.94 (t, *J* = 7.88 Hz, 1H), 7.09-7.13 (m, 2H), 7.38-7.43 (m, 2H), 7.52 (s, 1H), 7.56 (d, *J* = 8.44 Hz, 1H), 7.65-7.69 (m, 1H), 8.04 (d, *J* = 7.92 Hz, 1H). ^{13}C NMR (100 MHz, CD_3OD) δ 26.04, 38.10, 42.92, 55.75, 111.17, 118.46, 119.39, 119.43, 121.58, 122.25, 124.37, 124.63, 125.57, 127.89, 134.22, 136.56, 138.46, 152.80, 159.18, 163.20. MS (*m/z*) 413 (M^++1).

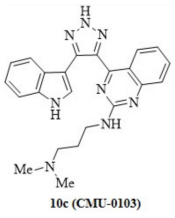

10c (CMU-0103)

4-(5-(5-fluoro-1H-indol-3-yl)-2H-1,2,3-triazol-4-yl)-2-(4-methylpiperazin-1-yl)quinazoline (10d, CMU-0104): Yield 87%, ^1H NMR (400 MHz, CD_3OD) *δ* 2.25 (s, 7H), 3.63 (brs, 4H), 6.89-6.98 (m, 2H), 7.22-7.26 (m, 1H), 7.38 (dd, *J* = 4.4 Hz, 4.4 Hz, 1H), 7.59 (s, 1H), 7.59 (s, 1H), 7.62 (s, 1H), 7.68-7.72 (m, 1H), 8.39 (dd, *J* = 0.4 Hz, 0.8 Hz, 1H). ^{13}C NMR (100 MHz, CD_3OD) *δ* 42.89, 44.64, 54.22, 104.23, 104.47, 104.59, 104.64, 109.81, 110.07, 112.09, 112.18, 117.88, 122.59, 125.39, 125.96, 126.07, 126.46, 127.45, 133.15, 133.84, 138.44, 139.77, 153.43, 156.84, 157.98, 159.16, 160.77. MS (*m/z*) 429 (M^++1).

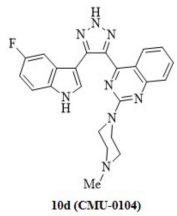

10d (CMU-0104)

4-(5-(5-methyl-1H-indol-3-yl)-2H-1,2,3-triazol-4-yl)-2-(4-methylpiperazin-1-yl)quinazoline (10e, CMU-0105): Yield 78%, ^1H NMR (400 MHz, $CDCl_3$) *δ* 2.23 (s, 10H), 3.65 (brs, 4H), 6.47 (brs, 1H), 6.88 (d, *J* = 8.8 Hz, 1H), 7.06-7.13 (m, 2H), 7.27 (s, 2H), 7.58 (d, *J* = 3.6 Hz, 2H), 8.35 (d, *J* = 8 Hz, 1H), 8.98 (brs, 1H). ^{13}C NMR (100 MHz, $CDCl_3$) *δ* 21.47, 29.71, 43.14, 45.49, 54.44, 104.63, 111.15, 118.21, 119.99, 122.91, 124.18, 124.83, 125.92, 127.82, 129.70, 134.00, 134.38, 139.18, 140.49, 153.50, 158.14, 160.63. MS (*m/z*) 425 (M^++1).

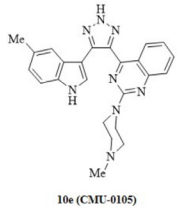

10e (CMU-0105)

Solvents and chemicals were purchased from the available commercial sources and used without further purification. Thin-layer chromatography was performed using pre-coated plates contained from E. Merck (TLC silica gel 60 F254). TLC plates were visualized by being exposed to ultraviolet light (UV). The column chromatography was performed on silica gel (200-400 mesh) using a mixture of ethyl acetate/hexane and methanol/dichloromethane as an eluent. The NMR spectra were recorded on Bruker AVANCE NEO 400 NMR spectrometer, and Mass spectra were measured on Liquid Chromatograph-Tandem Mass Spectrometer and Electrospray Ionization ESI method.

Statistical analysis

All experiments were repeated at least three times unless otherwise indicated. Error bars represent standard deviation (SD). Student's t test was used to compare two groups of independent samples. A *p* value < 0.05 was considered statistically significant.

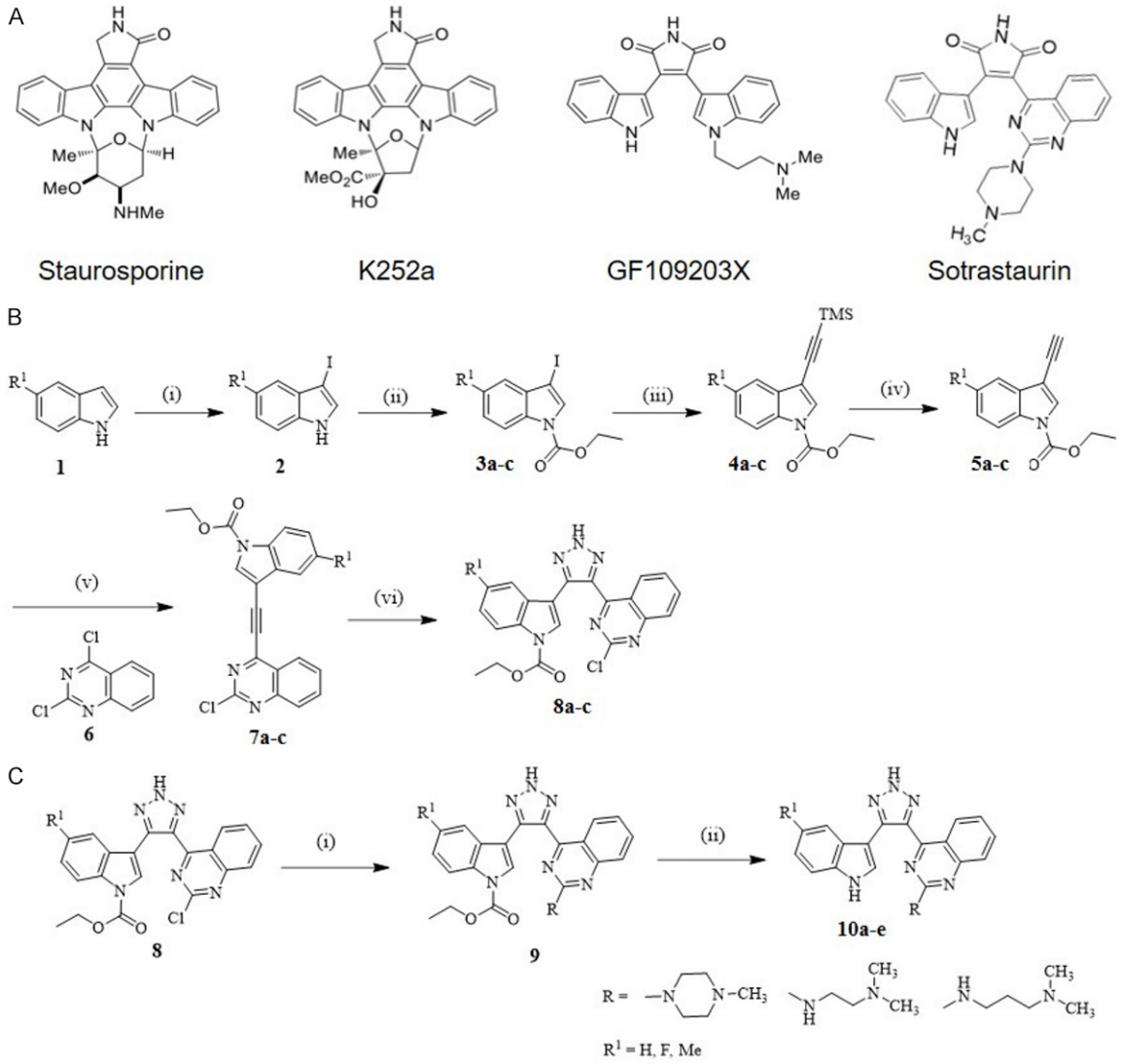

Figure 1. Synthetic scheme for triazole-based PKC inhibitors. A. Compound examples of bioactive indolocarbazole alkaloids, quinazolinones, and triazoles. B. Synthesis for heteroarylindolytriazole scaffolds. Reagents and conditions: (i) iodine, KOH, DMSO, 2 h; (ii) ethyl chloroformate, Et_3N, CH_2Cl_2, 0°C - rt, 3 h; (iii) trimethylsilylacetylene, $PdCl_2(PPh_3)_2$, CuI, Et_3N/DMF (5:1), 40°C, 1 h; (iv) 1.0 M Bu_4NF, THF, 0°C, 1 h; (v) 2,4-dichloroquinazoline, $PdCl_2(PPh_3)_2$, CuI, Et_3N/DMF (5:1), 40°C, 1 h; (vi) NaN_3, DMSO, rt, 3 h. C. Scope of primary aliphatic amines. Reagents and conditions: (i) *N*-methylpiperazine, 2-propanol, 100°C, 2 h, 79-82%; (ii) LiOH, MeOH, 12 h, rt, 86-91%.

Results

Heterocyclic scaffolds, which are organic compounds containing one or more rings with at least one non-carbon atom, are commonly used for designing protein kinase inhibitors [22]. These inhibitors mimic the structure of the adenine ring of adenosine triphosphate (ATP) and compete at the ATP-binding site of protein kinases, including PKC [22, 23]. Some examples of these scaffolds are indolocarbazole alkaloids, quinazolines, and triazoles [23]. Among them, indolocarbazole moiety is present in some well-known and commercially-available broad-spectrum PKC inhibitors, such as staurosporine, K252a, GF109203X, as well as sotrastaurin (**Figure 1A**). However, the ATP-binding pocket of PKC is highly conserved among different PKC isoforms and therefore, the heterocyclic scaffolds can potentially inhibit multiple PKC isoforms with similar binding sites. Modulating size of the heterocyclic moieties could assist in bringing selectivity.

We have previously demonstrated that treatment of sotrastaurin improved TKI resistance

in EGFR-mutant lung cancer in preclinical models [8]. However, sotrastaurin exhibits non-selectivity towards PKCδ and demonstrates a lower inhibitory efficacy for this isoform compared to other novel PKC isoforms, such as PKCθ (with Ki values of 2.1 nM for PKCδ and 0.22 nM for PKCθ) [24]. This may limit its efficacy and specificity for targeting nPKCδ in TKI-resistant tumors. Therefore, we sought to develop more potent inhibitors for PKCδ based on the structure of sotrastaurin. We aimed to improve the inhibitory efficacy of sotrastaurin for PKCδ, especially for nPKCδ which causes TKI resistance in lung cancer, by modifying its structure. Based on our experimental learning from sotrastaurin and other pan PKC inhibitors such as GF109203X (**Figure 1A**), we replaced the maleimide group of sotrastaurin with a triazole ring which is smaller and mimics hydrogen bond accepting properties of maleimide [25]. The preparation of the desired triazole-based PKCδ inhibitors is illustrated in **Figure 1B**. Iodination of indole followed by immediate methyl carbamate protection of the sensitive indole providing *N*-acetyl-3-iodoindole (1) with trimethylsilylacetylene under Sonogashira coupling in the presence of 20 mol% $Pd(PPh_3)_2Cl_2$, TEA:DMF (3:1) at reflux 1 h followed by cleavage of trimethylsillyl group using TBAF in THF to give *N*-acetyl-3-ethynylindole (5) [20]. The coupled with 2,4-dichloroquinazoline (6) using 20 mol% $Pd(PPh_3)_2Cl_2$, TEA:DMF (3:1) at reflux 3 h followed by workup to give quinazolineindole compound 7, which was using a [3+2] cycloaddition reaction with sodium azide, DMSO at room temperature for 3 h underwent smooth cycloaddition to afford a heteroarylindolytriazole (8) [21]. It then underwent nucleophilic aromatic substituted reaction with *N*-methylpiperazine to replace the chloro group to afforded the compounds 9 (79-82%) followed by hydrolysis of an ester using LiOH at room temperature for 12 h to afford the anticipated products 10 (CMU compounds) in 86-91% yields (**Figure 1C**). In this way, using the functionalized indole and quinazoline derivatives, we synthesized five triazole-based sotrastaurin derivatives CMU-0101, CMU-0102, CMU-0103, CMU-0104, and CMU-0105 as proof-of-concept PKC inhibitor candidates accordingly (**Figure 2A** and **2B**).

In our previous study, we generated several acquired gefitinib-resistant (GR) clones from EGFR-mutant HCC827 NSCLC cells by single-cell isolation [8]. We characterized these clones and found that they were highly resistant to three first-line TKIs, gefitinib, afatinib, and osimertinib, for EGFR-mutant NSCLC [8, 26]. We also discovered that all these clones generally exhibited nuclear translocation of PKCδ (nPKCδ), but not their parental cells. Inhibition of PKCδ by shRNA reversed TKI sensitivity in GR cells [8]. To test the most effective triazole-based PKC inhibitor candidates for sensitizing GR cells to TKIs, we performed a synthetic lethality screen using gefitinib with the five candidate inhibitors. We evaluated the cell viability of GR10 cells after treating them with gefitinib and each inhibitor for three days. Our analysis revealed that CMU-0101 was the most effective inhibitor in enhancing gefitinib-induced cell death in GR10 cells (**Figure 3A**) compared to other four derivatives (**Figure 3B-E**). To assess and compare the anti-cancer effects of CMU-0101 and sotrastaurin in TKI-resistant cells, we conducted a growth inhibitory analysis. Identical concentrations of CMU-0101 and sotrastaurin were administered, both with and without gefitinib. Our results revealed significant reductions in cell growth upon single treatment with CMU-0101 compared to sotrastaurin in both GR6 and GR10 cells (**Figure 4A** and **4B**). To explore the potential of CMU-0101 to enhance the anticancer activity of TKI in TKI-resistant cells, we performed a combination treatment study. GR6 and GR10 cells were exposed to combinations of CMU-0101/gefitinib and sotrastaurin/gefitinib, using identical concentrations of each compound. Cell killing activity was assessed via crystal violet staining. Our findings demonstrate that the CMU-0101/gefitinib combination exerts more potent growth inhibition compared to the sotrastaurin/gefitinib combination in both GR cell lines (**Figure 4B** and **4C**). To quantitatively evaluate the synergistic effects of the CMU-0101/gefitinib combination, we calculated the combination index (CI) employing the Chou-Talalay method (**Figure 4D**). CI serves as a numerical representation of the extent of synergy or antagonism between two drugs. A CI value below 1 signifies synergy, while a value equal to 1 indicates an additive effect, and a value above 1 suggests antagonism. Our results indicate that CMU-0101 treatment (at concentrations of 1-8 μM) synergistically enhances the anticancer potency of gefitinib in both GR6 and GR10 cells (**Figure 4D**, CI = 0.46-0.85 and 0.25-0.87, respectively).

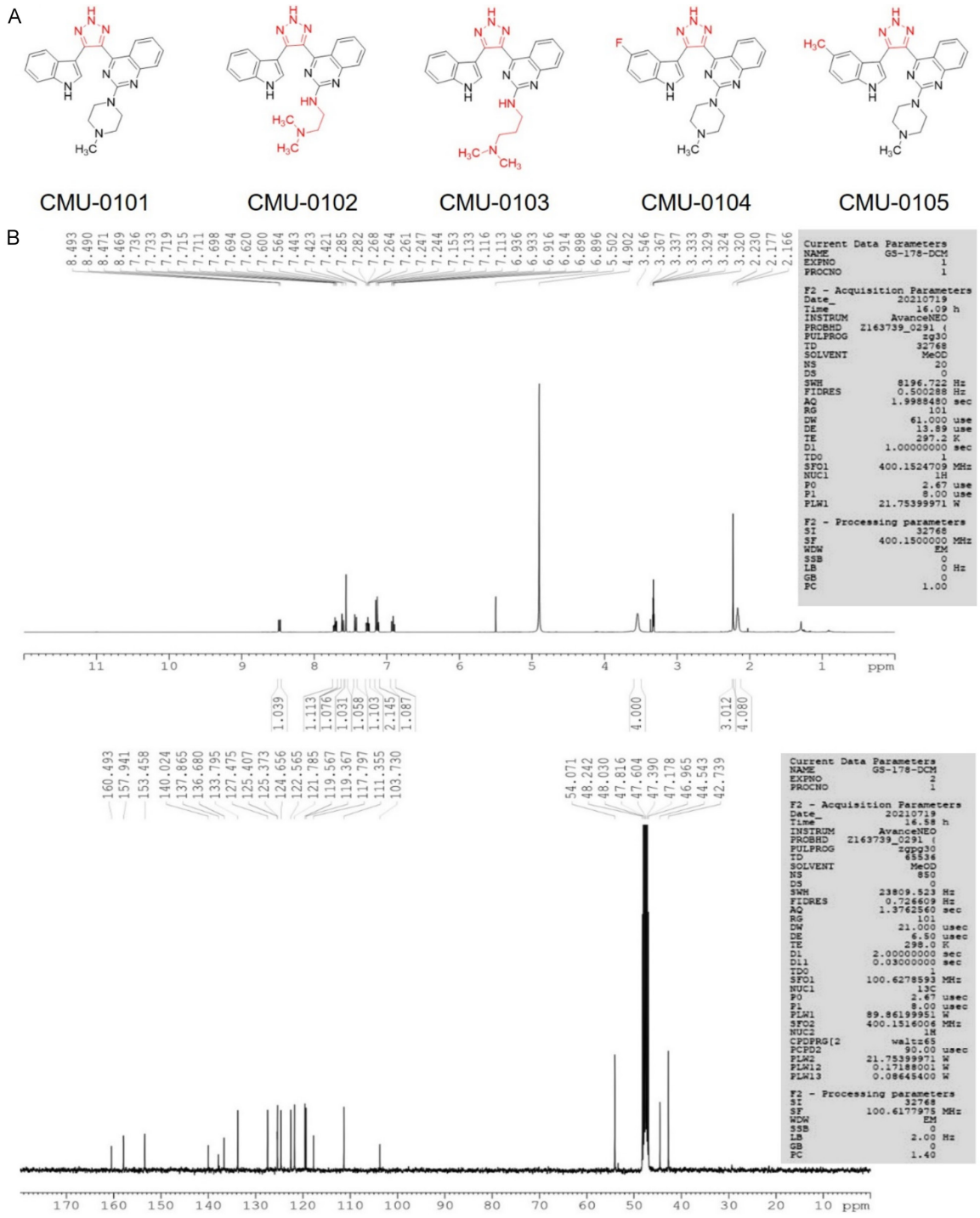

Figure 2. Five sotrastaurin derivatives. A. Chemical structures of CMU-0101, CMU-0102, CMU-0103, CMU-0104, and CMU-0105. B. ^{1}H (400 MHz, CD_3OD) and ^{13}C (100 MHz, CD_3OD) NMR spectra of CMU-0101.

Next, we tested whether our sotrastaurin derivatives that restored TKI sensitivity could inhibit nPKCδ in GR cells. We focused on CMU-0101, which showed the synergy with gefitinib in reducing GR cell viability. We treated GR10 cells with various concentrations of CMU-0101 or sotrastaurin for 24 h and stained the cells for PKCδ (**Figure 5A**). The stained cells were then analyzed by a confocal-based imaging system (ImageXpress Micro confocal system, Molecular

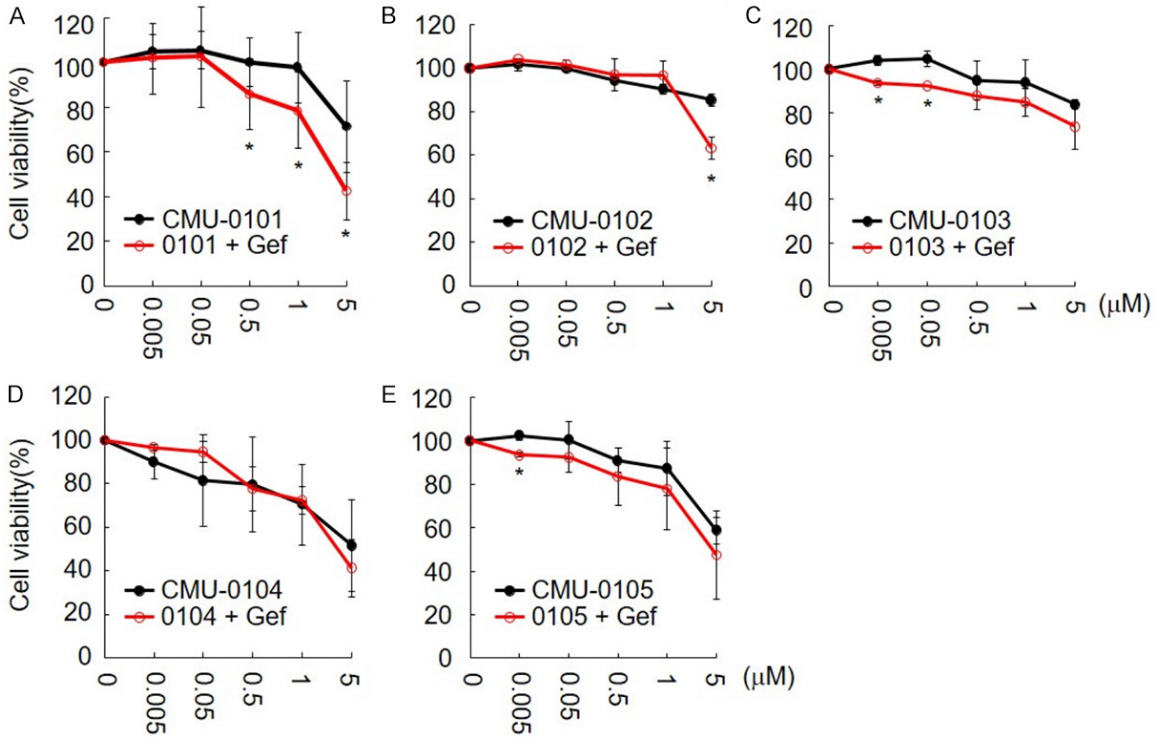

Figure 3. Synthetic lethality screen of gefitinib (gef) with five sotrastaurin derivatives in EGFR-mutant TKI-resistant lung cancer cells. Gefitinib-resistant (GR10) cells were treated with CMU-0101 (A), CMU-0102 (B), CMU-0103 (C), CMU-0104 (D), and CMU-0105 (E) at the indicated concentrations in combination with single dose gef (1 μM) for 3 days and subjected to cell viability assay by crystal violet staining. Data represent mean ± SD from at least three independent experiments. Comparisons between each single treatment groups with its combination group were analyzed using Student's t test. *P < 0.05.

Devices) that automatically focuses on nuclear level of the cells, captures multiple images per well, and quantifies the nuclear intensity of PKCδ staining. Our results showed that CMU-0101 suppressed nPKCδ in a dose-dependent manner (**Figure 5B**). Moreover, at 20 μM, CMU-0101 was significantly more effective than sotrastaurin in inhibiting nPKCδ (**Figure 5B**). Furthermore, we conducted an extensive evaluation of nuclear PKCδ (nPKCδ) expression through western blot analysis. This evaluation encompassed both nuclear extracts (NE) and cytoplasm extracts (CE) of GR cells subjected to CMU-0101 treatment. Our findings indicated a dose-dependent reduction in nuclear PKCδ levels in both GR6 and GR10 cells upon exposure to CMU-0101 (**Figure 5C**). To assess the selectivity of CMU-0101 towards PKCδ, we examined its inhibitory effects on the activation statuses of both PKCδ and three additional PKC isoforms, all 4 PKCs belonging to the novel PKC subfamily. To conduct this evaluation, we treated GR10 cells with CMU-0101 and subsequently subjected the cell lysates to Western blot analysis. During this analysis, we employed specific antibodies targeting the phosphorylation of PKCδ, PKCε, PKCη, and PKCθ in order to discern their activation statuses. Our results confirmed that CMU-0101 treatment suppressed the phosphorylation of PKCδ (**Figure 5D**). Interestingly, this suppression had no observable impact on the activation of the other three novel PKC isoforms, namely ε, η, and θ (**Figure 5D**). These results suggest that CMU-0101 demonstrates a relatively selective influence on PKCδ. Together, these data indicated that CMU-0101 is a potent inhibitor of nPKCδ and a potential drug candidate for overcoming TKI resistance in NSCLC cells.

To understand how our novel inhibitor CMU-0101 inhibits PKCδ, we used molecular docking, a computational technique that predicts how a small molecule binds to a protein target. We analyzed the docking poses (**Figure 6A** and **6B**) and binding energy (**Figure 6C**) of CMU-0101 and sotrastaurin for PKCδ. The result indicated that PKCδ has higher affinity to CMU-

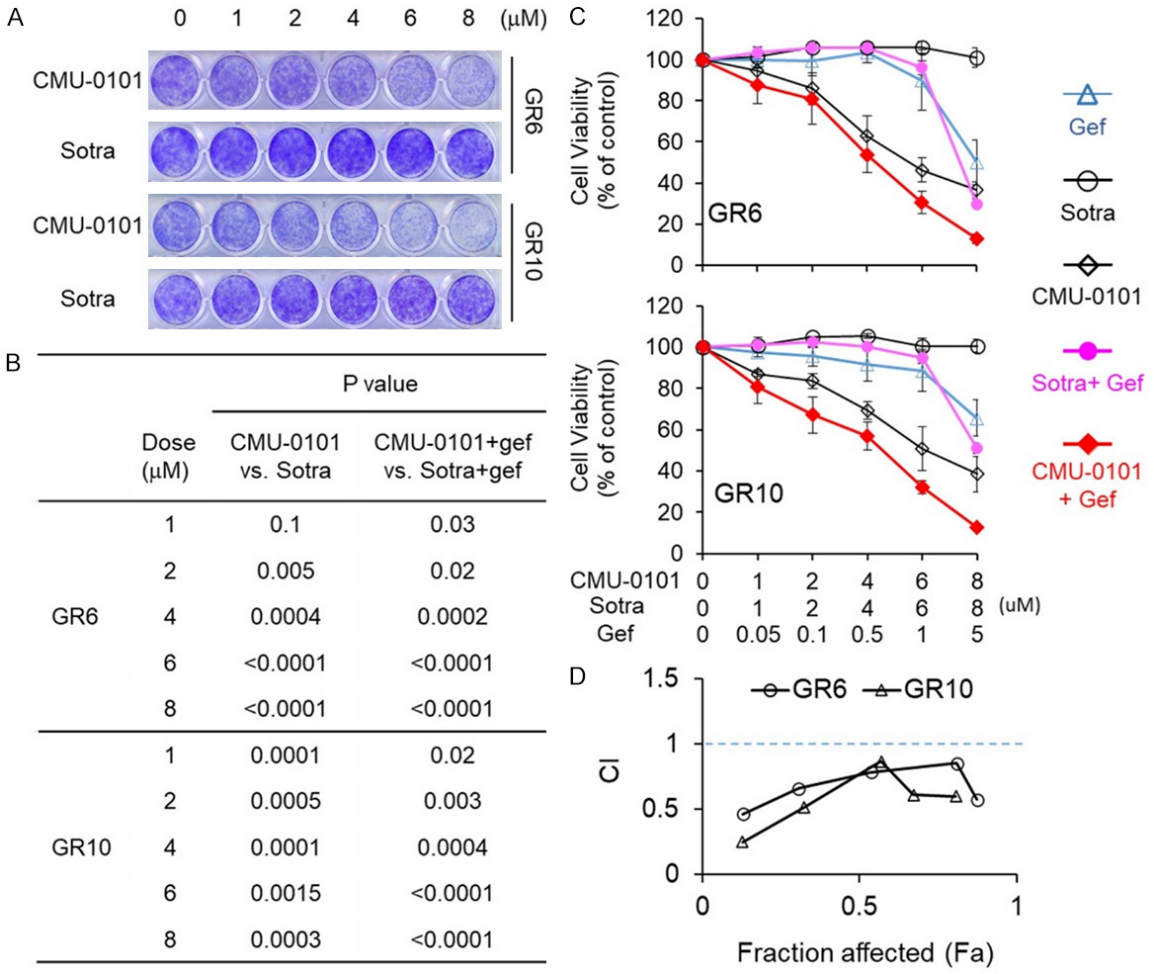

B

	Dose (μM)	P value: CMU-0101 vs. Sotra	P value: CMU-0101+gef vs. Sotra+gef
GR6	1	0.1	0.03
	2	0.005	0.02
	4	0.0004	0.0002
	6	<0.0001	<0.0001
	8	<0.0001	<0.0001
GR10	1	0.0001	0.02
	2	0.0005	0.003
	4	0.0001	0.0004
	6	0.0015	<0.0001
	8	0.0003	<0.0001

Figure 4. Synergistic effects of CMU-0101 with gefitinib in TKI-resistant cells. (A) Dose response of CMU-0101 and sotrastaurin (sotra) in GR6 and GR10 cells. (B) *P*-values indicating statistical significances of cell growth inhibition at indicated concentrations. Comparisons between CMU-0101 and sotra treatment groups were analyzed using Student's t test. (C) Combination effects of gefitinib (gef) with CMU-0101 and sotra in GR6 and GR10 cells. The cells were treated with CMU-0101 and sotra in combination with gef at the indicated concentrations for 6 days. Cell viability was assayed by crystal violet staining. (D) Quantitation of CMU-0101 and gef from (C) with drug combination indexes (CI). CI < 1, synergy; CI = 1, additive; CI > 1.1, antagonism.

0101 than sotrastaurin, meaning that CMU-0101 associates more strongly with the ATP-binding pocket of PKCδ. This finding was further supported by the total number of formed hydrogen bonds, which are important for stabilizing the ligand-protein interaction. While sotrastaurin formed a single hydrogen bond with the backbone of PKCδ residue K357 (**Figure 6A**), CMU-0101 formed two hydrogen bonds with N478 and D491 (**Figure 6B**). These data suggest that PKCδ prefers CMU-0101 over sotrastaurin in terms of energy-driven binding. Interestingly, despite the structural similarity of CMU-0101 and sotrastaurin, the docking result shows that PKCδ binds to these two inhibitors with different poses (**Figure 6A** and **6B**). Together, our findings support that our chemical modification strategy of sotrastaurin is effective to produce more hydrogen bonds with nearby acceptors, enhance binding affinity to PKCδ, and inhibit nPKCδ in the resistant cells.

Discussion

Although PKC has been associated with various diseases, it constitutes a diverse family of at least 12 isoforms, each carrying out distinct functions and exhibiting different tissue distributions [27]. Initially, PKC isoforms were perceived as oncogenes that drive cancer growth

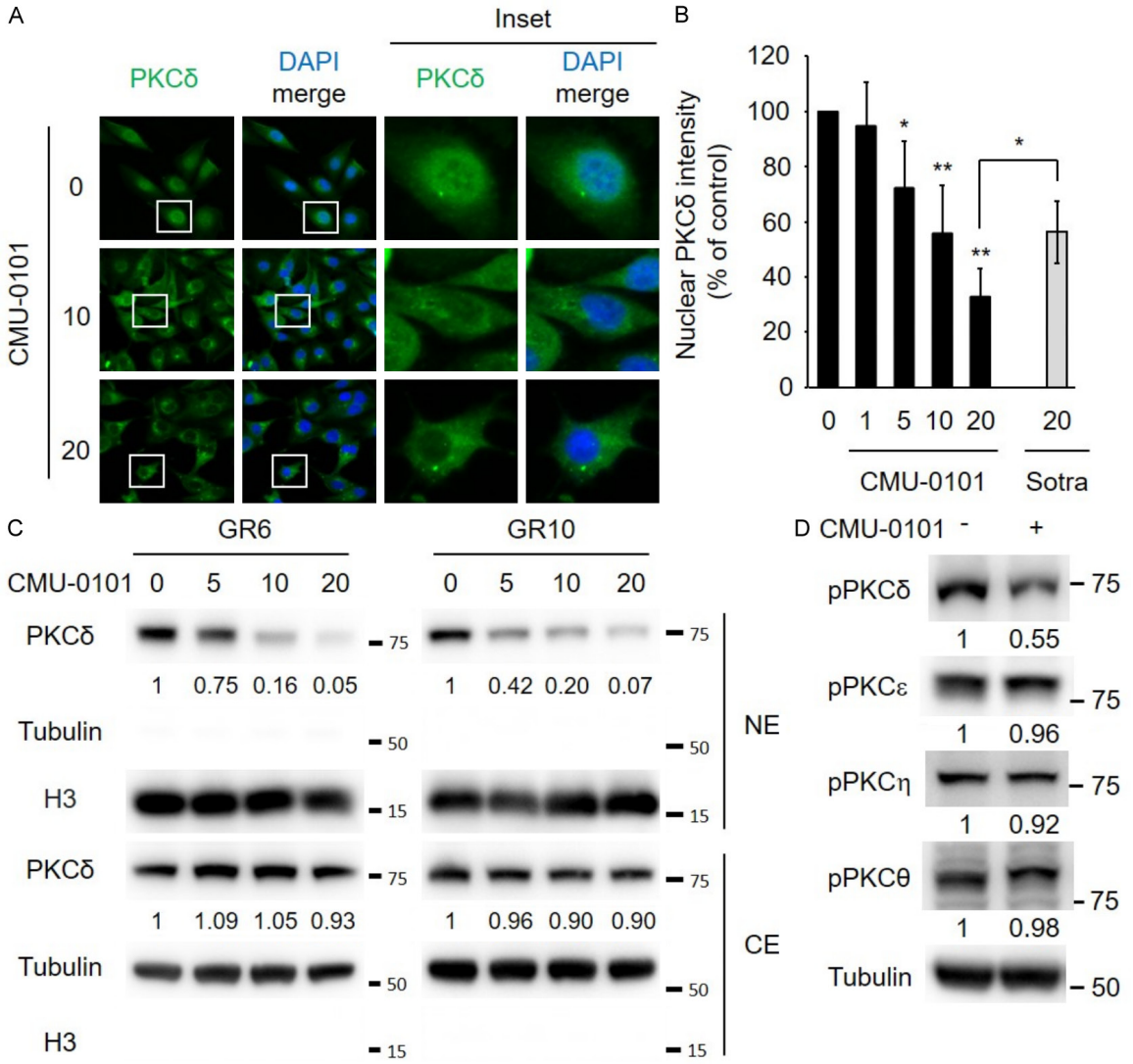

Figure 5. Inhibition of PKCδ by CMU-0101. A. Confocal microscopy analysis of PKCδ nuclear localization in GR10 cells by immunofluorescence staining (green). The cells were treated with CMU-0101 for 24 h and subjected to immunofluorescence staining for PKCδ (green). Nuclei were counterstained with DAPI (blue). B. Quantification analysis of nPKCδ expression in GR10 cells treated with CMU-0101 and sotrastaurin (sotra) at the indicated concentrations. ImageXpress Micro confocal system analyzed fluorescence intensity of PKCδ in nuclei of GR10 cells after the treatments. C. PKCδ expression by western blot analysis in both nuclear extracts (NE) and cytoplasm extracts (CE) of GR6 and GR10 cells treated with CMU-0101 for 24 h. Relative PKCδ levels are indicated below the blot. D. Western blot analysis of phosphorylation of PKCδ, PKCε, PKCη, and PKCθ in GR10 cells treated with CMU-0101 (20 μM) for 24 h. Relative expression levels are indicated below the blot.

and survival. However, subsequent research uncovered loss-of-function mutations in specific PKC isoforms within tumors, revealing their role as tumor suppressors by inhibiting cancer formation and dissemination [28, 29]. The dual or opposing roles of PKC isoforms appear to be contingent upon their unique regulation and expression patterns, displaying a cell-type dependency. Notably, PKCδ, one such isoform, has been identified as overexpressed or activated across various cancer types. Within EGFR-mutant lung cancers, our research underscores PKCδ's role as an oncogene, fostering resistance to TKIs [8].

Strategically inhibiting protein kinases, such as PKCδ, by competing with their binding to ATP, emerges as a promising approach for treating relevant cancers. The adenine ring, a pivotal component of ATP, engages with several residues at the base of the PKC catalytic domain's ATP-binding pocket [30]. Consequently, the

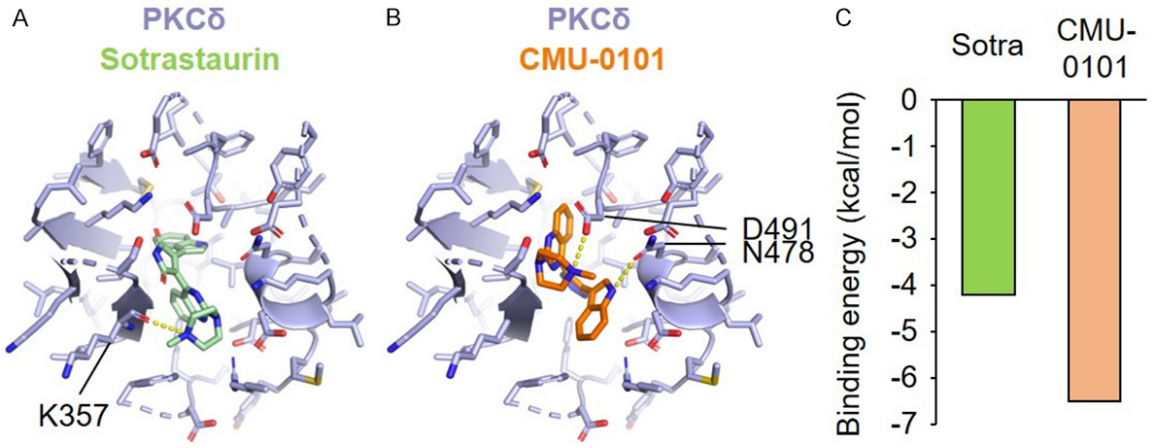

Figure 6. Molecular docking analysis of sotrastaurin and CMU-0101 with PKCδ ATP-binding site (A-C). (A) 3D visualization of sotrastaurin binding to PKCδ, forming a single hydrogen bond with K357. (B) 3D visualization of CMU-0101 binding to PKCδ, forming two hydrogen bonds with N478 and D491. Hydrogen bonds are shown as yellow dashed lines. (C) Binding energy of sotrastaurin (sotra) and CMU-0101 with PKCδ.

design of PKC inhibitors often involves heterocyclic compounds mimicking the adenine ring. These compounds obstruct PKC activation by disrupting ATP binding to the ATP-binding domain of PKC [22, 23]. However, it's noteworthy that the ATP-binding domain is conserved across diverse PKC isoforms, rendering most commercially available drugs non-selective towards any specific isoform. This can potentially lead to undesired effects in cancer patients due to the varying roles of PKC isoforms in cancer development and progression [31].

To confer selectivity, modifying existing pan-PKC inhibitors to augment their binding affinity to PKCδ stands as a rational and pragmatic strategy. Our chemical modification approach, exemplified by CMU-0101, involved introducing a triazole ring group into sotrastaurin, thereby reducing the maleimide moiety from 4.5 Å to 2.3 Å. This alteration is speculated to empower CMU-0101 with the capacity to explore more potential binding poses within the ATP-binding pocket of PKCδ. Subsequently, it can find the optimal pose for interaction with surrounding residues, a feature markedly distinct from sotrastaurin. Indeed, our results demonstrated that CMU-0101 exhibits a considerably stronger binding affinity to PKCδ's ATP-binding site than sotrastaurin. This suggests CMU-0101's potential efficacy in inhibiting PKCδ by competing ATP binding. Demonstrating its impact, CMU-0101 treatment effectively suppressed nPKCδ in TKI-resistant cells and synergistically collaborated with EGFR TKI to suppress cell growth. Therefore, our data showed a promising strategy for synthesizing and developing potential PKC inhibitors and supported that CMU-0101 is a leading compound for treating EGFR-mutant TKI-resistant lung cancers.

Acknowledgements

We acknowledge the supports of initial idea and guidance by Dr. Ching-Shih Chen. This work was supported by China Medical University, Taiwan (YingTsai Young Scholar Award CMU-108-YTY-03 and CMU110-IP-03 to P.C.L.), National Science and Technology Council, Taiwan (MOST 109-2314-B-039-058-MY2 to P.C.L.; NSTC 111-2311-B-039-002 to Y.C.L.; NSTC 112-2639-B-039-001-ASP to M.C.H.), Ministry of Health and Welfare Taiwan (MOHW-112-TDU-B-222-124016 to M.C.H.). This work was financially supported by the "Cancer Biology and Precision Therapeutics Center, China Medical University" from The Featured Areas Research Center Program within the framework of the Higher Education Sprout Project by the Ministry of Education (MOE) in Taiwan. This work was also partially supported by the grants CMU108-Z-07, CMU109-Z-07 and CMU110-Z-07 from China Medical University, and Drug Development Center, China Medical University from The Featured Areas Research Center Program within the framework of the Higher Education Sprout Project by the Ministry of Education (MOE) in Taiwan.

Disclosure of conflict of interest

None.

Address correspondence to: Mien-Chie Hung and Pei-Chih Lee, Graduate Institute of Biomedical Sciences, China Medical University, No. 100, Sec. 1, Jingmao Rd., Beitun Dist., Taichung, Taiwan. Tel: +886-4-22057153; Fax: +886-4-22952121; E-mail: mhung@cmu.edu.tw (MCH); Tel: +886-4-22053366; Fax: +886-4-22060248; E-mail: antiolde333@gmail.com (PCL); Hsiang-Wen Lin and Chih-Shiang Chang, School of Pharmacy, College of Pharmacy, China Medical University, Taichung, Taiwan. Tel: +886-4-22053366; E-mail: hsiangwl@gmail.com (HWL); chihshiang@mail.cmu.edu.tw (CSC)

References

[1] Skoulidis F and Heymach JV. Co-occurring genomic alterations in non-small-cell lung cancer biology and therapy. Nat Rev Cancer 2019; 19: 495-509.

[2] Marusyk A, Janiszewska M and Polyak K. Intratumor heterogeneity: the Rosetta stone of therapy resistance. Cancer Cell 2020; 37: 471-484.

[3] Cooper AJ, Sequist LV and Lin JJ. Third-generation EGFR and ALK inhibitors: mechanisms of resistance and management. Nat Rev Clin Oncol 2022; 19: 499-514.

[4] Nie L, Wang YN, Hsu JM, Hou J, Chu YY, Chan LC, Huo L, Wei Y, Deng R, Tang J, Hsu YH, Ko HW, Lim SO, Huang K, Chen MK, Chiu TJ, Cheng CC, Fang YF, Li CW, Goverdhan A, Wu HJ, Lee CC, Wang WL, Hsu J, Chiao P, Wang SC and Hung MC. Nuclear export signal mutation of epidermal growth factor receptor enhances malignant phenotypes of cancer cells. Am J Cancer Res 2023; 13: 1209-1239.

[5] Saab S, Chang OS, Nagaoka K, Hung MC and Yamaguchi H. The potential role of YAP in Axl-mediated resistance to EGFR tyrosine kinase inhibitors. Am J Cancer Res 2019; 9: 2719-2729.

[6] Steen NV, Potze L, Giovannetti E, Cavazzoni A, Ruijtenbeek R, Rolfo C, Pauwels P and Peters GJ. Molecular mechanism underlying the pharmacological interactions of the protein kinase C-beta inhibitor enzastaurin and erlotinib in non-small cell lung cancer cells. Am J Cancer Res 2017; 7: 816-830.

[7] Matkar S, An C and Hua X. Kinase inhibitors of HER2/AKT pathway induce ERK phosphorylation via a FOXO-dependent feedback loop. Am J Cancer Res 2017; 7: 1476-1485.

[8] Lee PC, Fang YF, Yamaguchi H, Wang WJ, Chen TC, Hong X, Ke B, Xia W, Wei Y, Zha Z, Wang Y, Kuo HP, Wang CW, Tu CY, Chen CH, Huang WC, Chiang SF, Nie L, Hou J, Chen CT, Huo L, Yang WH, Deng R, Nakai K, Hsu YH, Chang SS, Chiu TJ, Tang J, Zhang R, Wang L, Fang B, Chen T, Wong KK, Hsu JL and Hung MC. Targeting PKCdelta as a therapeutic strategy against heterogeneous mechanisms of EGFR inhibitor resistance in EGFR-mutant lung cancer. Cancer Cell 2018; 34: 954-969, e954.

[9] Sos ML, Koker M, Weir BA, Heynck S, Rabinovsky R, Zander T, Seeger JM, Weiss J, Fischer F, Frommolt P, Michel K, Peifer M, Mermel C, Girard L, Peyton M, Gazdar AF, Minna JD, Garraway LA, Kashkar H, Pao W, Meyerson M and Thomas RK. PTEN loss contributes to erlotinib resistance in EGFR-mutant lung cancer by activation of Akt and EGFR. Cancer Res 2009; 69: 3256-3261.

[10] Bivona TG, Hieronymus H, Parker J, Chang K, Taron M, Rosell R, Moonsamy P, Dahlman K, Miller VA, Costa C, Hannon G and Sawyers CL. FAS and NF-kappaB signalling modulate dependence of lung cancers on mutant EGFR. Nature 2011; 471: 523-526.

[11] Sandhu S, Bansal Y, Silakari O and Bansal G. Coumarin hybrids as novel therapeutic agents. Bioorg Med Chem 2014; 22: 3806-3814.

[12] Chou TC. Theoretical basis, experimental design, and computerized simulation of synergism and antagonism in drug combination studies. Pharmacol Rev 2006; 58: 621-681.

[13] Lee PC, Lee HJ, Kakadiya R, Sanjiv K, Su TL and Lee TC. Multidrug-resistant cells overexpressing P-glycoprotein are susceptible to DNA crosslinking agents due to attenuated Src/nuclear EGFR cascade-activated DNA repair activity. Oncogene 2013; 32: 1144-1154.

[14] Jumper J, Evans R, Pritzel A, Green T, Figurnov M, Ronneberger O, Tunyasuvunakool K, Bates R, Zidek A, Potapenko A, Bridgland A, Meyer C, Kohl SAA, Ballard AJ, Cowie A, Romera-Paredes B, Nikolov S, Jain R, Adler J, Back T, Petersen S, Reiman D, Clancy E, Zielinski M, Steinegger M, Pacholska M, Berghammer T, Bodenstein S, Silver D, Vinyals O, Senior AW, Kavukcuoglu K, Kohli P and Hassabis D. Highly accurate protein structure prediction with AlphaFold. Nature 2021; 596: 583-589.

[15] Tunyasuvunakool K, Adler J, Wu Z, Green T, Zielinski M, Zidek A, Bridgland A, Cowie A, Meyer C, Laydon A, Velankar S, Kleywegt GJ, Bateman A, Evans R, Pritzel A, Figurnov M, Ronneberger O, Bates R, Kohl SAA, Potapenko A, Ballard AJ, Romera-Paredes B, Nikolov S, Jain R, Clancy E, Reiman D, Petersen S, Senior AW, Kavukcuoglu K, Birney E, Kohli P, Jumper J and Hassabis D. Highly accurate protein structure prediction for the human proteome. Nature 2021; 596: 590-596.

[16] Li YC, Yamaguchi H, Liu YY, Hsu KC, Sun TH, Sun PC and Hung MC. Structural insights into EphA4 unconventional activation from prediction of the EphA4 and its complex with ribonuclease 1. Am J Cancer Res 2022; 12: 4865-4878.

[17] Wagner J, von Matt P, Sedrani R, Albert R, Cooke N, Ehrhardt C, Geiser M, Rummel G, Stark W, Strauss A, Cowan-Jacob SW, Beerli C, Weckbecker G, Evenou JP, Zenke G and Cottens S. Discovery of 3-(1H-indol-3-yl)-4-[2-(4-methylpiperazin-1-yl)quinazolin-4-yl]pyrrole-2,5-dione (AEB071), a potent and selective inhibitor of protein kinase C isotypes. J Med Chem 2009; 52: 6193-6196.

[18] Eberhardt J, Santos-Martins D, Tillack AF and Forli S. AutoDock Vina 1.2.0: new docking methods, expanded force field, and python bindings. J Chem Inf Model 2021; 61: 3891-3898.

[19] Wallace AC, Laskowski RA and Thornton JM. LIGPLOT: a program to generate schematic diagrams of protein-ligand interactions. Protein Eng 1995; 8: 127-134.

[20] Oakdale JS and Boger DL. Total synthesis of lycogarubin C and lycogalic acid. Org Lett 2010; 12: 1132-1134.

[21] Tsai CW, Yang SC, Liu YM and Wu MJ. Microwave-assisted cycloadditions of 2-alkynylbenzonitriles with sodium azide: selective synthesis of tetrazolo[5,1-a]pyridines and 4,5-disubstituted-2H-1,2,3-triazoles. Tetrahedron 2009; 65: 8367-8372.

[22] Sherer C and Snape TJ. Heterocyclic scaffolds as promising anticancer agents against tumours of the central nervous system: exploring the scope of indole and carbazole derivatives. Eur J Med Chem 2015; 97: 552-560.

[23] Heravi MM and Zadsirjan V. Prescribed drugs containing nitrogen heterocycles: an overview. RSC Adv 2020; 10: 44247-44311.

[24] Evenou JP, Wagner J, Zenke G, Brinkmann V, Wagner K, Kovarik J, Welzenbach KA, Weitz-Schmidt G, Guntermann C, Towbin H, Cottens S, Kaminski S, Letschka T, Lutz-Nicoladoni C, Gruber T, Hermann-Kleiter N, Thuille N and Baier G. The potent protein kinase C-selective inhibitor AEB071 (sotrastaurin) represents a new class of immunosuppressive agents affecting early T-cell activation. J Pharmacol Exp Ther 2009; 330: 792-801.

[25] Salameh BA, Abu-Safieh KA, Al-Hushki EH, Talib WH, Al-ataby IA and Al-Qawasmeh RA. New maleimide 1,2,3-triazole hybrids: design, synthesis, anticancer, and antimicrobial activities. Monatshefte Fur Chemie 2020; 151: 1609-1619.

[26] Hong X, Hsieh MT, Tseng TY, Lin HY, Chang HC, Yau ST, Cheng WC, Ke B, Liao HH, Wu CY, Liu AA, Wu MM, Huang KY, Yang PC, Kuo SC, Hung MC and Lee PC. Diarylheptanoid 35d overcomes EGFR TKI resistance by inducing hsp70-mediated lysosomal degradation of EGFR in EGFR-mutant lung adenocarcinoma. J Biol Chem 2023; 299: 104814.

[27] Parker PJ, Brown SJ, Calleja V, Chakravarty P, Cobbaut M, Linch M, Marshall JJT, Martini S, McDonald NQ, Soliman T and Watson L. Equivocal, explicit and emergent actions of PKC isoforms in cancer. Nat Rev Cancer 2021; 21: 51-63.

[28] Antal CE, Hudson AM, Kang E, Zanca C, Wirth C, Stephenson NL, Trotter EW, Gallegos LL, Miller CJ, Furnari FB, Hunter T, Brognard J and Newton AC. Cancer-associated protein kinase C mutations reveal kinase's role as tumor suppressor. Cell 2015; 160: 489-502.

[29] Mochly-Rosen D, Das K and Grimes KV. Protein kinase C, an elusive therapeutic target? Nat Rev Drug Discov 2012; 11: 937-957.

[30] Kumar V, Weng YC, Geldenhuys WJ, Wang D, Han X, Messing RO and Chou WH. Generation and characterization of ATP analog-specific protein kinase Cdelta. J Biol Chem 2015; 290: 1936-1951.

[31] Deka SJ and Trivedi V. Potentials of PKC in cancer progression and anticancer drug development. Curr Drug Discov Technol 2019; 16: 135-147.